A New Multiparameter Approach to Computational Simulation for Fontan Assessment and Redesign

Alison L. Marsden, PhD,* V. Mohan Reddy, MD,† Shawn C. Shadden, PhD,‡
Frandics P. Chan, MD, PhD,§ Charles A. Taylor, PhD,§¶** and Jeffrey A. Feinstein, MD, MPH¶**

*Mechanical and Aerospace Engineering Department, University of California, San Diego, †Department of Cardiothoracic Surgery, Stanford University, Stanford, Calif., ‡Department of Mechanical, Materials and Aerospace Engineering, Illinois Institute of Technology, Chicago, IL, §Department of Radiology, ¶Department of Pediatrics, **Department of Bioengineering, Stanford University, Stanford, Calif., USA

ABSTRACT

Introduction. Despite an abundance of prior Fontan simulation articles, there have been relatively few clinical advances that are a direct result of computational methods. We address a few key limitations of previous Fontan simulations as a step towards increasing clinical relevance. Previous simulations have been limited in scope because they have primarily focused on a single energy loss parameter. We present a multi-parameter approach to Fontan modeling that establishes a platform for clinical decision making and comprehensive evaluation of proposed interventions.

Methods. Time-dependent, 3-D blood flow simulations were performed on six patient-specific Fontan models. Key modeling advances include detailed pulmonary anatomy, catheterization-derived pressures, and MRI-derived flow with respiration. The following performance parameters were used to rank patients at rest and simulated exercise from best to worst performing: energy efficiency, inferior and superior vena cava (IVC, SVC) pressures, wall shear stress, and IVC flow distribution.

Results. Simulated pressures were well matched to catheterization data, but low Fontan pressure did not correlate with high efficiency. Efficiency varied from 74% to 96% at rest, and from 63% to 91% with exercise. Distribution of IVC flow ranged from 88%/12% (LPA/RPA) to 53%/47%. A "transcatheter" virtual intervention demonstrates the utility of computation in evaluating interventional strategies, and is shown to result in increased energy efficiency.

Conclusions. A multiparameter approach demonstrates that each parameter results in a different ranking of Fontan performance. Ranking patients using energy efficiency does not correlate with the ranking using other parameters of presumed clinical importance. As such, current simulation methods that evaluate energy dissipation alone are not sufficient for a comprehensive evaluation of new Fontan designs.

Key Words. Fontan Surgery; Patient-Specific Modeling; Hemodynamics; Exercise; Computational Fluid Dynamics

Introduction

Some of the earliest work in computational fluid dynamics applied to congenital heart disease compared energy loss in the standard "t" junction Fontan with the proposed "offset" model, and led to the adoption of the offset model as the currently preferred method.[1–4] Since that time a decade ago, there has been ongoing, and recently growing, interest in modeling the Fontan circulation. This interest coupled with increases in computational power have led to the development of more sophisticated computational tools and increasingly physiologically realistic simulations.[4–7]

Despite the increasing sophistication of simulations, most studies to date still focus solely on the "engineering" aspects of the problem and few have succeeded in applying simulation strategies to realistic clinical scenarios. This is due to several factors. First, there has been a lack of validation and/or outcomes studies incorporating simulation-based parameters. And second, previous Fontan modeling has often been limited in

scope, with restrictive anatomical models, nonphysiologic pressure levels, and a single parameter approach to evaluating performance. For example, much of the previous modeling work has not been validated against pressures from catheterization despite the fact that pressure plays a key role in clinical decision making for Fontan patients. Additionally, energy loss (or a surrogate thereof) has been the parameter examined almost exclusively, while additional parameters of potential clinical importance[8–12] have not been evaluated. While energy loss (or Fontan efficiency) is likely linked to clinical outcomes, it would be a gross oversimplification to assume it to be the sole determinant of a Fontan's success or failure. A recent review article of DeGroff[13] issued a "call to arms" to increase the sophistication and impact of Fontan simulations by including, among other things, respiration, exercise, wall compliance, unsteady flow, and more accurate anatomy.

In an attempt to address some of the above concerns and move to broaden the clinical applicability of Fontan simulations, this article takes a new multiple-parameter approach to Fontan modeling. Using patient-specific models derived from image data, we perform comprehensive simulations of six Fontan patients at rest and under simulated exercise conditions. For each patient, we evaluate energy efficiency, inferior vena cava (IVC) and superior vena cava (SVC) pressure levels, wall shear stress (WSS) and quantify distribution of IVC flow to the left and right pulmonary arteries. For each of these parameters, patients are ranked in order of best to worst performing. The modeling advances used in this work include more detailed pulmonary anatomy, respiration, exercise, particle tracking methods, and sophisticated boundary conditions that achieve physiologic pressure levels.

As an example, a "transcatheter" virtual intervention is performed on one of the six patients and its performance is evaluated with respect to its baseline and the other subjects. The intervention performed is a virtual stent placement to correct for left pulmonary artery (LPA) compression. The goal of this approach is to lay a foundation for future optimization, clinical validation, and evaluation of new treatment strategies for Fontan patients.

Methods

The general schema of patient-specific modeling involves image and clinical (e.g., catheterization) data acquisition, anatomic model construction, flow simulation, and postprocessing to produce performance measures, such as flow distribution and Fontan pressure, that are surrogates for known predictors of patient outcomes. Virtual interventions were performed in two of six patients by altering the anatomic models to represent the proposed intervention. All patients were imaged and catheterized as part of their routine clinical care and their data were used with Stanford and University of California, San Diego institutional review board approval. Methods for all of the above steps are summarized in the remainder of this section; additional technical details of the simulations are presented in greater depth in the Appendix. The authors had full access to the data and take responsibility for their integrity. All authors have read and agree to the manuscript as written.

Six patients (5 female) ranging in age from 3 to 26 years status post extracardiac Fontan procedure were included in this study. None of the patients were fenestrated. Relevant demographic and clinical data are shown in Table 1.

Image Acquisition

Magnetic Resonance Imaging

Magnetic resonance angiography for patients A–E was performed on a 1.5 Tesla MRI scanner (Signa

Table 1. Relevant Clinical Data for the Six Patients (A–F) Used in This Study. The Age and BSA Are at the Time of Image Acquisition. The Inferior Vena Cava (IVC), Left and Right Pulmonary Artery (LPA, RPA), PA Pressures, Cardiac Index (CI) and Pulmonary Wedge Pressure (PCW) Are Obtained from Cardiac Catheterization

Patient	Age/Sex	BSA (mm^2)	IVC_p (mm Hg)	SVC_p (mm Hg)	LPA_p (mm Hg)	RPA_p (mm Hg)	CI (cath) ($L/min/m^2$)	PCW (mm Hg)
A	17/F	1.55	18	18	17	17	2.3	11
B	26/F	1.65	15	15	14	14	1.6	12
C	3/M	0.68	11	11	10	10	3.8	5
D	3/F	0.67	7	7	6	6	2.8	3
E	6/F	0.71	9	9	6	6	2.7	4
F	5/F	0.68	11	11	7	9	2.8	3

Twin-Speed, General Electrics, Milwaukee, WI). During intravenous administration of gadolinium-based contrast agent, images were acquired using 3-D fast gradient-recalled echo sequence with the patient in breath-hold. The spatial resolution was approximately 0.7 mm × 1.2 mm × 2.0 mm. Flow information in the IVC was recorded using a 2-D MRI phase-contrast (PCMRI) method. The imaging plane was placed perpendicular to the dominant flow in the IVC and velocity encoding parallel to the flow. The slice thickness was 10 mm and the in-plane resolution was about 1.0 mm × 1.7 mm. The maximum encoded velocity was 120 cm/s. Data were acquired over several cycles of free breathing using cardiac gating and respiratory compensation. The IVC flow was interrogated mid baffle.

Computed Tomography

MRI was attempted for patient F, but due to the presence of too much metal artifact, computer tomography angiography was performed on a 16-slice multidetector row CT (Sensation 16, Siemens, Forchheim, Germany). During intravenous administration of iodinated x-ray contrast agent, thin-section spiral scan of the chest was acquired with breath-hold and reconstructed at 1 mm slice thickness. The in-plane resolution was about 0.4 mm × 0.4 mm.

Model Construction

Model construction for all patients was performed directly from the MRI or CT image data using a customized version of the Simvascular open source software package (available from http://simtk.org).[14,15] The pulmonary vasculature model included all pulmonary branches of size greater than or equal to the segmental branches, representing the resolution limits of the image data. The outlets represented all of the major branches of the LPA and right pulmonary artery (RPA). Models were constructed with the following steps: (1) paths were defined that run down the center of the vessels of interest, (2) the vessel lumen was defined at fixed intervals along each vessel (segmented), (3) the vessel portions between the two-dimensional segmentations were interpolated and joined using custom software to create a 3-D solid model of the desired vasculature (lofted), and (4) a mesh was generated to represent the solid model for use in the finite element flow solver.

The steps in model construction are illustrated in Figure 1 for patient E. Figure 2 shows the final models for all six patients.

Blood Flow Simulations and Inflow Boundary Conditions

For each of the six patients, blood flow simulations were performed at rest and two levels of simulated exercise. A 3-D Navier-Stokes solver (also part of the Simvascular open source project) was employed with a rigid-wall approximation. More details on the simulation methods and flow solver can be found in the Appendix. Each simulation was run on 20–24 processors of an SGI Altix parallel

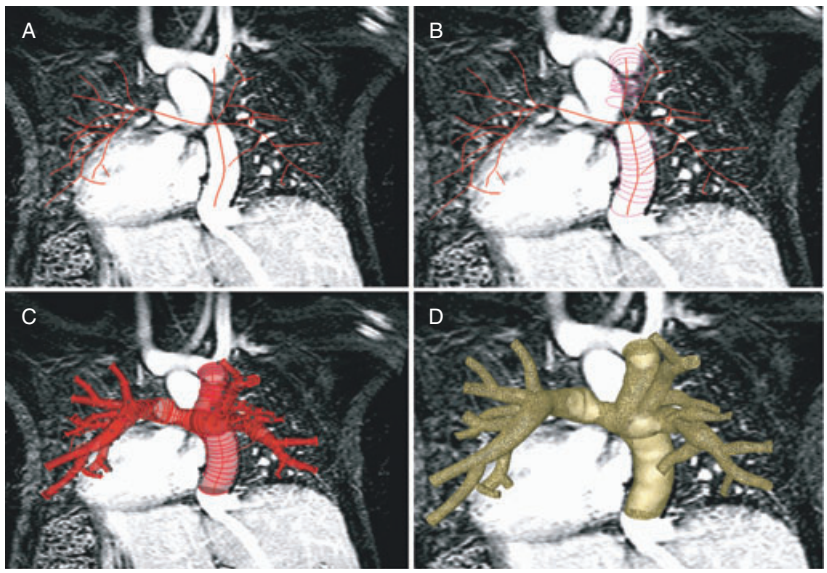

Figure 1. Four steps involved in model construction (patient D) are (A) creation of vessel paths (B) segmentation (C) lofting, and (D) mesh generation. Image is displayed in the posterior-anterior view for ease of viewing.

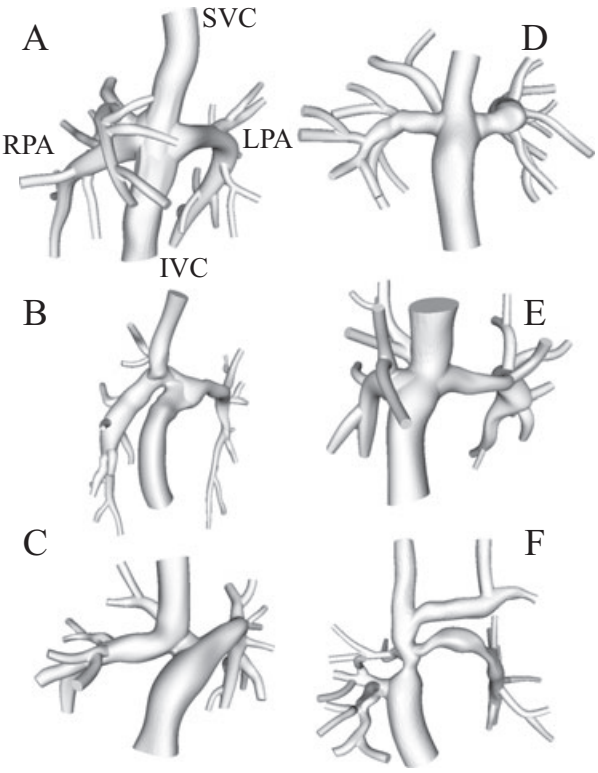

Figure 2. Anatomic models for 6 Fontan patients A–F. (5 female, ages 3–26) Large geometric variation is observed among patients. Patient E has a significant LPA stenosis, patient F has since undergone a surgical revision.

supercomputer, requiring about 1000 CPU hours (two days) of run time. Simulation results were postprocessed to produce velocity, pressure, and WSS information throughout the model.

Inflow boundary conditions at the SVC and IVC at rest were derived from PCMRI data. For all patients, it was ensured that the total flow rates (IVC + SVC) were within 15% of the flow predictions measured in catheterization using Fick's method. For patient F, who had CT imaging, a typical waveform was used and scaled to the patient's body surface area.

Exercise and Respiration

Three mean flow rates were used in the IVC: normal/resting (i.e., measured) flow, and two and thre times normal flow to simulate exercise conditions. These values were chosen based on clinical exercise data in Fontan patients, in which on average, Fontan patients are able to approximately double their cardiac index at peak exercise.[16,17]

Cardiac catheterization pressure tracings, echocardiography, and MR studies have all demonstrated that respiration significantly affects Fontan flow rates and pressures.[18,19] As seen with the echocardiographic tracings, quantitative real-time phase contrast MR measurements by Hjortdal et al.[18] show that flow rates in the IVC vary significantly with respiration at rest (as much as 80%), with smaller cardiac pulsatility superimposed. Cardiac variations in the SVC were found to be small, with no significant respiratory variation. Based on these data, we impose a respiration model to model flow variations in the IVC following our previously published work.[6] The pulsatile SVC inflow was derived from the MRI data with no additional respiration model.

Large variations in IVC flow rate with respiration are consistent with the concept of peripheral venous capacitance.[18,20] The large venous capacitance in the lower body allows for blood accumulation during expiration, and release of stored blood during inspiration. The smaller SVC respiratory variation is explained by a lower venous capacitance in the upper body. As mean IVC flow rates increase with exercise, the amplitude of respiratory variation remains relatively constant, which is likely attributed to an effective venous pump created by an increase in blood flow due to lower body muscle activity.

The respiratory model consists of a simple two-part polynomial model with input variables corresponding to respiratory rate, inspiratory fraction (the percentage of time spent during inspiration), inspiratory and expiratory mean flow rates, and fraction of retrograde flow. The respiratory model has a mean of zero and is superimposed on the waveform generated by PCMRI to generate the final IVC flow waveform.

A ratio of three cardiac cycles per respiratory cycle was assumed throughout. With this assumption, a reasonable range of respiratory rates (21–45) and heart rates (63–135) for rest and exercise cases are obtained. Our previous work using this model demonstrated good qualitative agreement between predicted LPA pressures and pressure tracings obtained in cardiac catheterization.

Outflow Boundary Conditions

Outflow boundary conditions were imposed at all outlets using the coupled multidomain method[21] with a lumped parameter 3-element Windkessel model.[22] The first step in assigning parameters for the lumped model was to choose initial downstream resistance values to match patient-specific cardiac catheterization pressure data for each patient (Table 1). Initial LPA/RPA flow splits were assumed to be 45/55. If needed, flow splits were

adjusted after an initial simulation was run to match pressure drops to the LPA and RPA measured during catheterization for each patient and to match flow rates measured in the LPA and RPA using PCMRI.

On each side (LPA and RPA), flow was distributed among the pulmonary outlets by grouping them into upper, middle, and lower lobes. Initial resistances were chosen to distribute 20% of the flow to the upper lobe and 40% each to the middle and lower lobes. For lack of other data, these values were based on the assumption that each of the 10 major lung segments receives equal flow. Within each lobe group, flow was distributed according to the outlet areas. The number of outlets in each group varied among patients, with 2–3 outlets in the upper lobes, and 3–5 outlets in each of the middle and lower lobes. The total number of pulmonary branches included in the simulations varied from 19 to 21. An initial steady simulation was run for each model using resistance boundary conditions to verify that catheterization pressure data were matched within 0.5 mm Hg in the IVC and SVC.

The initial resistance values were then used to generate a morphometry-based pulmonary arterial tree[23] for each outlet of the model. The resistance and capacitance parameters in the lumped model for each outlet were optimized so that the impedance of the lumped model best fit the impedance of the morphometry-based pulmonary arterial tree. To simulate exercise, the morphometry-based arterial trees were dilated and the resistance values were decreased by 5% and 10% for the two levels of exercise based on clinical observations that pulmonary vascular resistance in both normal children and Fontan patients decreases with exercise.[16,24]

Energy Efficiency

Energy efficiency was calculated for each model at rest and all exercise levels by calculating the rate of energy passing through all inlets and outlets.[25] Energy efficiency defined in this manner does not consider the effects of abnormalities of the microvasculature or left heart parameters. While most previous work has used mean values of velocity and pressure on the model faces to compute energy loss,[2,6,7,26] a recent article by Grigioni et al.[27] demonstrated significant errors can arise using this method. Therefore, we use the exact integral on each face of the model in the present study (see Appendix). The efficiencies we report in this work are time-averaged over one respiratory cycle. Convergence studies confirmed results did not change using multiple respiratory cycles. The equations used to compute efficiency can be found in the appendix.

Inferior Vena Caval Flow Distribution

Specialized methods to "virtually track" particles have been recently developed and applied to cardiovascular problems.[28] These methods were applied to quantify the distribution of IVC flow to the right and left pulmonary arteries. Particles were introduced in the IVC, and their course through the Fontan circuit tracked until they exited the model. Approximately two respiratory cycles were required for nearly all particles to exit the model. From a technical standpoint, the distribution of the IVC flow to the LPA and RPA can be largely influenced by model geometry while the overall flow distribution (SVC + IVC) to the LPA and RPA is mostly determined by the outflow boundary conditions.

The proportion of IVC flow going to the left lung was quantified by summing the number of particles that exited the model through outlets connected to the LPA. Likewise, the portion of IVC flow to the right lung was quantified by summing the number of particles that exited through outlets connected to the RPA. It was verified that the results were independent of the seeding density and rate, and the integration error tolerance.

Virtual Interventions

A virtual intervention was performed on one of the six patients (patient E), and results were examined in the context of all six patients. Patient E was found to have a severe LPA stenosis due to compression by the reconstructed aorta causing a 3 mm Hg pressure drop to both the LPA and RPA. (see Figure 2) To predict whether a stent would reduce energy losses for this patient, we virtually expanded the LPA to 9 mm to simulate stent placement. This was done using the same modeling tools that were used to create the original model from image data. Simulations were performed on the modified geometry keeping all other conditions, including inflow and outlet boundary conditions and pulmonary anatomy, the same. We then compute the pre- and postintervention energy efficiency, using the original geometry as a baseline for comparison. In addition, we compare with the efficiency results for all other patients to provide a context for evaluating the magnitude of efficiency changes.

Results

Fontan Geometry and Hemodynamics

Figure 2 shows the models for all six patients. We observe that geometry varies dramatically among patients in this study. Patients A, D, and E have Fontan connections with little or no offset of the IVC relative to the SVC. Patient E has a significant LPA stenosis. Patients B and C have pronounced offsets of the IVC to the LPA side, our current, standard surgical approach. Patient F has a double LPA stenosis, and a significant narrowing at the connection point between the IVC and SVC. This patient has since been sent for a surgical revision. We also observe large variations in pulmonary architecture among the six patients. In patients B, C, and E, the right upper lobe connects directly to the SVC. In patient D, the right upper lobe is connected at the junction between the IVC and SVC. The model geometries are all in good qualitative agreement with the anatomy observed by angiography during catheterization.

Pressure levels in the IVC and SVC at rest and two levels of simulated exercise are shown in Figure 3. The values shown are time-averaged over one respiratory cycle. Pressure levels increase for all patients during exercise, but the rise is more pronounced for patients A and C. We note that these two patients both had high resting Fontan pressures (15 in patient C and 18 mm Hg in patient A), were older (17 and 26), and had ventricular dysfunction and heart failure symptoms.

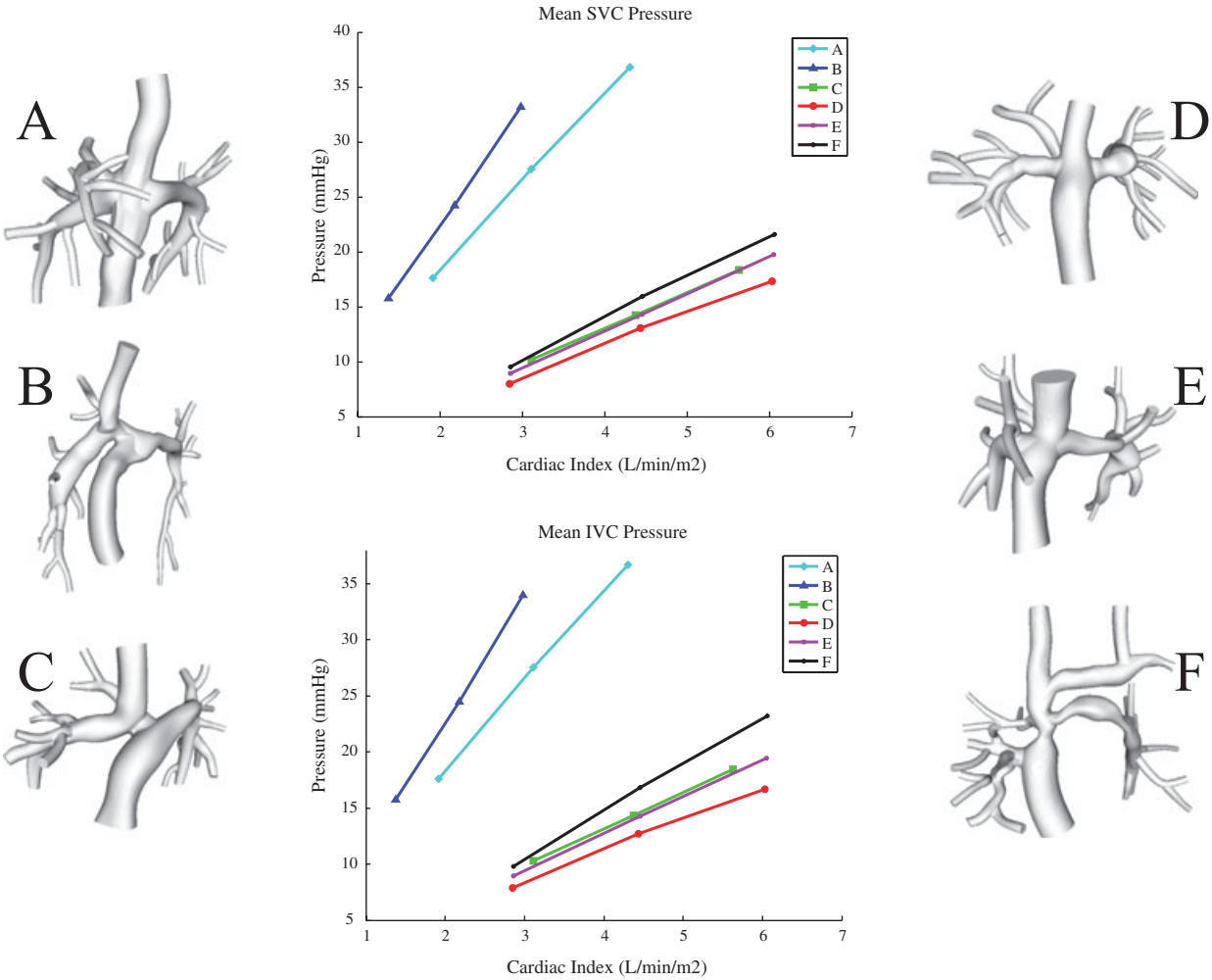

Figure 3. Pressure levels (mm Hg) in the SVC (upper) and IVC (lower) for each of the six patients in the study at rest (first data point) and exercise (2×—second point, 3×—third point). Pressures rises substantially with exercise. The two patients with the greatest increase in both relative and absolute pressure (A and B) both had high PCW, ventricular dysfunction and heart failure. Values are time-averaged over one respiratory cycle.

Table 2. Ranking of Fontan Performance from Best (Top) to Worst (Bottom) According to Multiple Competing Objectives (i.e., "Cost Functions")

Rank	Rest SVC_p	Exercise SVC_p	Rest Effic.	Exercise Effic.	Mean WSS	IVC Flow Distr.
Best	D	D	A	A	C	D
	E	C	B	B	F	A
	F	E	C	C	B	B
	C	F	D	E	A	F
	B	B	E	D	E	E
Worst	A	A	F	F	D	C

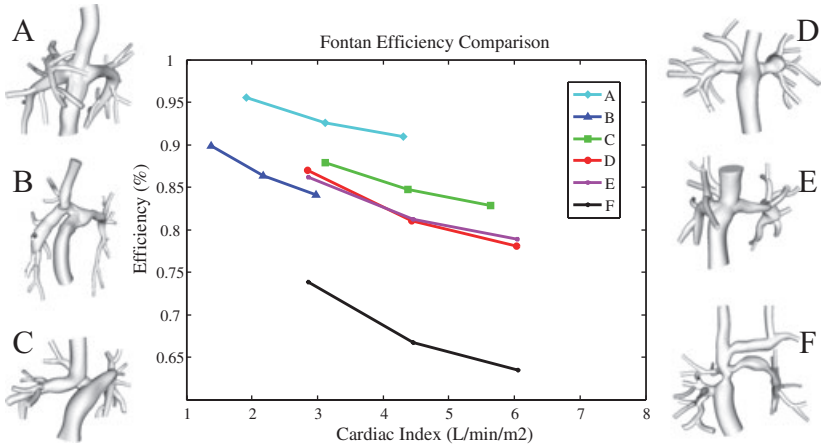

Figure 4. Comparison of Fontan efficiency (energy losses) for 6 patients in this study at rest (point 1) and exercise (2×—point 2, 3×—point 3). All patients show a decline in efficiency with exercise. Values are time-averaged over one respiratory cycle.

Pressure levels for the other four patients were 7–11 mm Hg at rest and rose to 15–20 mm Hg with a tripling of cardiac output during exercise. The ranking of patients from lowest (best) to highest (worst) SVC pressure is shown in Table 2 for rest and exercise.

Pressure drops to the LPA and RPA in the simulations are in good agreement with values measured during catheterization shown (Table 1). Patient F had a 2 mm Hg gradient in the proximal LPA and another 2 mm Hg gradient in the distal LPA.

Energy Efficiency

Energy efficiency is used to compare and rank the performance of the six geometries considered in this study. Results are summarized in Figure 4. As would be expected, the data show a substantial drop in efficiency with increasing exercise level for all six patients. Efficiency at rest ranges from 74% to 96% and at exercise (3× cardiac output) from 63% to 91%. Patient A had the highest efficiency at both rest and exercise, while patient F had the lowest efficiency. The mean rest to exercise drop in efficiency for all patients was 7 percentage points, with the largest being a 10 percentage point drop for patient F, and the smallest being a 5 point drop for patient A. The ranking of patients in order of most (best) to least (worse) efficient at rest and exercise is shown in Table 2.

Inferior Vena Caval Flow Distribution

The distribution of IVC flow to the right and left lungs is presumed to be important for delivery of a hepatic factor carried in IVC blood. Table 3 quantifies the distribution of IVC flow to the LPA and RPA using the particle tracking method. The table compares the distribution of IVC blood flow (column 2) to the overall flow distribution (IVC + SVC, column 3) for each patient. The distribution of total flow is enforced by the outflow boundary conditions for each patient, and does not depend directly on the connection geometry. The data demonstrate that the IVC flow split can differ dramatically from the total flow split. For example, patients B and C both have a nearly even overall flow split, but IVC flow is biased toward the LPA side (the side of the offset) by as much as 88%.

Table 3. Distribution of IVC Flow to the Left Pulmonary Artery (LPA) and Right Pulmonary Artery (RPA) during Resting Flow Conditions for All Six Patients

Fontan Patient	% IVC Flow to LPA/RPA	% Total Flow to LPA/RPA
A	35/65	45/55
B	70/30	43/57
C	88/12	45/55
D	53/47	45/55
E	16/84	30/70
F	22/78	38/62

Patients E and F both have severe LPA stenoses with an overall flow split that favors the right side. In both of these patients, IVC flow is even more strongly skewed to the right PA compared with the total (IVC + SVC) flow. Table 2 ranks the patients in order, where a distribution closer to 50/50 is (arbitrarily) assumed better and further from 50/50 is assumed worse. It is expected that SVC flow distribution is also affected by geometry, and would be the inverse of the IVC flow distribution, resulting in the total flow (IVC + SVC) distribution to each side.

WSS

Figure 5 shows the mean WSS values (dynes/cm^2) for all six models over one respiratory cycle during resting flow conditions. Minimum and mean (in space) shear stress values on the graft (IVC) portion of each model are given in Table 4. In general, areas of lowest wall shear are found in the IVC and SVC and near the Fontan junction. We note that the two patients (A and B) with lower overall wall shear (including the PA's) are the two with the highest resting energy efficiency. We also observe areas of high shear in stenotic regions (particularly in patients E and F) where velocities are increased. Patients are ranked in order of highest (best) to lowest (worst) mean wall shear on the graft portion in Table 2. This ranking was chosen based on observations that low WSS and areas of flow recirculation are linked to formation of thrombosis[29] and atherosclerosis.[30–32]

Virtual Intervention

The efficiency results for the virtual intervention was examined in the context of the group of six subjects. Results (patient E) demonstrate increases in efficiency at rest and exercise. Figure 6 compares the efficiency pre- and poststent for patient E. Efficiency is improved from 86% to 90% at rest and from 77% to 84% at heavy exercise. In comparison to the other six patients, the insertion of the stent improves the ranking of patient E from fifth to second at rest and from fourth to second with exercise.

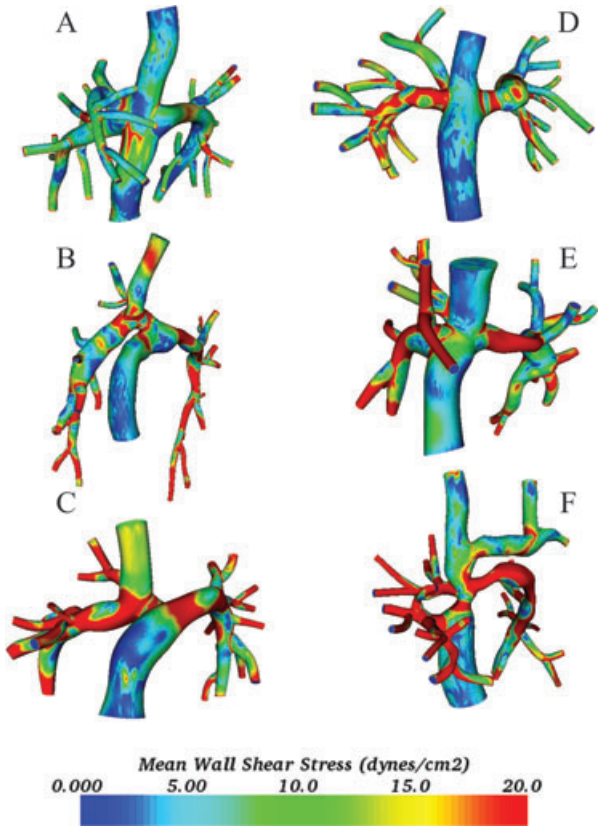

Figure 5. Contours of mean wall shear stress (dynes/cm^2) at rest for the six subjects in the study. Values are time-averaged over one respiratory cycle.

Table 4. Minimum and Mean (in Space) Wall Shear Stress (WSS) Values over the Graft Portion of the Model Only. Values Are the Average over One Respiratory Cycle during Resting Flow Conditions

Fontan Patient	Minimum WSS on Graft (dyne/cm^2)	Mean WSS on Graft (dyne/cm^2)
A	0.22	7.0
B	0.30	7.7
C	0.20	15.3
D	0.15	3.6
E	0.49	6.5
F	0.39	7.8

Discussion

In this study, we have evaluated the performance of six patients using multiple cost functions, including WSS, flow distribution, energy loss, and Fontan pressure levels during rest and exercise.

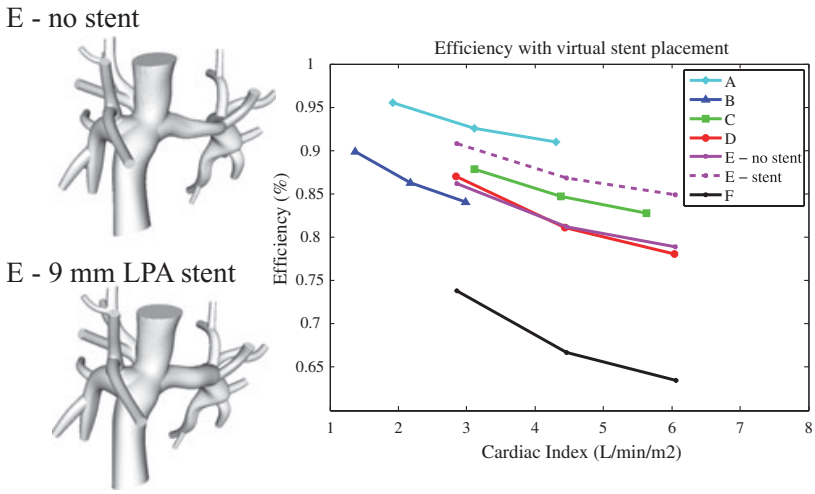

Figure 6. Efficiency improvement in patient E after virtual stent placement to correct LPA stenosis. Efficiencies for all six patients in the study are shown.

We summarize our results in Table 2, which demonstrates that each of these parameters produces a different ranking when ordering patients from best to worst performance. These results demonstrate that a single simulation-based parameter (such as energy dissipation) is not likely to hold all the answers to improving Fontan performance and that a multiple parameter approach is needed in future engineering and clinical evaluation of Fontan patients. In addition, predictions based on geometric efficiency without incorporation of patient-specific physiology and additional parameters may lead to generalizable knowledge but will likely not be useful as a clinical tool. The multiple-parameter approach illustrates that we still do not know what a good or bad Fontan is, and that we will not have a quantitative answer to that question until we account for multiple parameters and validate them against clinical outcomes.

This work has demonstrated several key modeling advances that improve the clinical relevance of Fontan modeling tools compared with previous work. We have, at least partially, addressed several of the key concerns raised in a recent review article by DeGroff[13] by including respiration, exercise, unsteady flow, particle tracking, and detailed pulmonary anatomy. We have incorporated sophisticated pulmonary boundary conditions that allow for physiologic levels of pressure and have validated our predicted pressure drops with catheterization data.

The concept of multiple competing cost functions are the norm in many other design and optimization problems. For example, in aeronautics, competing objectives such as lift, drag, weight, and structural strength are balanced in identifying an optimal airplane wing design. Similarly, the relative importance of cost functions for a Fontan patient may depend on individual risk factors or clinical symptoms, such as history of a clotting disorder, unequal LPA and RPA sizes, high resting Glenn pressure, etc. From a computation standpoint, we have now reached a point where simulations, incorporating patient-specific data, have the potential to function as another diagnostic tool in the ongoing evaluation of Fontan patients and proposed surgical or transcatheter revisions. Detailed comparisons between multiple cost functions such as those discussed here and clinical outcomes need to be made to close the loop between simulations and clinical practice. In the future, competing objectives should be considered in designing an optimal treatment plan for each patient rather than making decisions on a one-size-fits-all basis.

Pressures

Currently, Fontan pressure levels are used as a primary measure for clinical decision making. It is well accepted that Fontan pressures should be kept low whenever possible, and that outcomes are generally more favorable, though not universally good, for patients with lower pressures. Our results demonstrate that even patients with very low Fontan pressures may have high energy loss and inefficiencies. For example, patients D and E both had low resting Fontan pressures (9 and 7 mm Hg) but ranked 4th and 5th out of six

patients in efficiency performance at rest. In addition, patients with high efficiency may have a large pressure rise during exercise. In the two older patients (A and B) who had clinical symptoms of ventricular dysfunction with or without symptoms of heart failure, the simulated pressure levels rose dramatically to around 25–28 mm Hg with a doubling of cardiac output. While these pressure levels are admittedly very high for a Fontan patient, right atrial pressures in the range of 25 mm Hg have been observed clinically during catheterization of Fontan patients during exercise.[16] These results also suggest that if one were to compare two patients, one child and one adult, with the same high resting Fontan pressure, that the adult will experience a higher exercise pressure than the child, assuming they both double their cardiac output during exercise. This is an area that should be examined in future studies.

Energy Efficiency

Previous simulations of Fontan hemodynamics have reported very low energy dissipation values,[2,33,34] leading to the belief among some there is little room for improvement in Fontan performance. However, our work has demonstrated that Fontan efficiencies can be as low as 60–70% for some patients and there is a significant drop in efficiency for all patients with exercise. Our results showing that efficiencies decrease with exercise agree with previous simulation work.[7] We have also demonstrated (as with patients D and E) that designs that are superior at rest may not be superior at exercise. These findings agree with observations well known in the fluid mechanics community, that the characteristics of the flow (including vortex shedding, presence of stagnated flow, etc.) can change dramatically with increasing flow rate.

We should note that the efficiencies reported here are patient-specific values for a given body size and cardiac output. As such, the result that patient A (a t-junction) was the most efficient cannot be taken to mean that the t-junction is the most efficient design for all patients. It is quite possible that modifying the geometry of patient A to an offset, for example, could further improve efficiency for that patient. Efforts to improve energy efficiency by modifying Fontan geometry should use patient-specific modeling and optimization.

WSS

Clinical studies have shown that anticoagulation (either with aspirin or coumadin) improves outcomes postoperatively for Fontan patients and that the incidence of thrombus formation at varying locations is 10–20% regardless of the type of Fontan surgery.[11,35] It is currently not known what level of WSS is linked to higher risk of thrombosis, and to determine this requires stronger links with biological data. Simulation tools can provide a valuable way to predict shear stress. However, one must be careful drawing conclusions about geometries using a single metric. For example, one could make a reasonable assumption that a lower *mimimum* WSS value would correspond to a higher risk of thrombosis in the graft (Table 4). This might lead us to the following ranking of patient risk (from lowest to highest risk): E, F, B, A, C, D. However, it may be equally reasonable to assume that the lower *mean* WSS in the graft corresponds to higher risk, leading to a very different ranking: C, F, B, A, E, D (Table 2). Future work should examine the size of low WSS areas, as well as particle residence time and WSS gradients in attempt to correlate with patient outcomes, platelet adhesion data, and thromboses.

IVC Flow Distribution

The development of arteriovenous malformations has been linked in previous studies[10,36] to the lack of a presumed hepatic factor that is essential for lung development. While it is not known what concentration is required for normal lung development, it is clear that the distribution of IVC flow to the right and left PAs will impact the concentration of hepatic factor present in the lungs. Additionally, one could assume if all other factors are equal, it would be desirable to distribute the flow as evenly as possible. Our results demonstrate that IVC flow distribution is dramatically affected by Fontan geometry. Offset geometries, such as observed in patients B and C, strongly skew the IVC flow to one side over another, even if the overall LPA/RPA flow split is close to 50/50. Patients E and F both had a pronounced LPA stenosis, and IVC flow in these patients was strongly skewed to the right side. While the overall flow distribution is determined by the downstream resistance, the distribution of IVC flow is highly dependent on geometry and the type of Fontan connection. Related results in our previous study on a new Y-graft modification of the Fontan indicate that the Y-graft design distributes the IVC flow much more evenly than offset designs.[25] These results provide additional motivation for new surgical designs, such as the Y-graft, which distribute the IVC flow more evenly between the two lungs.

Virtual Interventions

We have demonstrated the use of simulation for examining changes in efficiency after a virtual stent implantation to relieve an LPA stenosis caused by compression by the reconstructed aorta. In the future, interventions chould be evaluated on multiple-patient models and correlated with short- and long-term clinical outcomes. It would be essential to balance improvements in efficiency as a result of stent placement against risk of thrombus formation as a result of the stent. Despite the improvements demonstrated in simulations, we make no claim that interventions should be performed soley based on simulations. A significant amount of work both in the realm of validation and application remains before these techniques are universally accepted and employed. Another example of a virtual surgery application can be found in our recent work on the Y-graft Fontan modification.[25]

Limitations

There are several limitations to this study that should be considered. One limitation of this study is the use of rigid walls, although recent work has demonstrated success of new and efficient fluid-structure interaction algorithms[37–39] that should be incorporated into future work on Fontan modeling. Another limitation is the lack of patient data for flow distribution among the pulmonary lobes and for the response of pulmonary resistances to exercise. Previous work has proposed alternate normalizations for energy dissipation.[7,40] Different metrics should be continued to be explored in future work. In this work, energy efficiency is compared for models with approximately the same number of pulmonary outlets and extent of branching. However, efficiency values for a given patient model will change with the addition or removal of more levels of pulmonary branching. An additional challenge for clinical implementation in large patient populations is the time intensive nature of model building and simulations.

Conclusions

Using six patient-specific computational models, we have evaluated multiple Fontan performance metrics at rest and exercise (energy efficiency, flow distribution, pressure levels, and WSS) and demonstrated that patient rankings differ widely depending on which metric is used for evaluation. This result strongly suggests that there is no single parameter that is the sole determinant of a Fontan's success or failure but that Fontan treatment decisions should be made using a multiple-parameter approach. Our results have demonstrated that that there is substantial room for improvement in Fontan hemodynamics for some patients and that patients with high energy efficiency are not necessarily the patients with low Fontan pressures. The huge range of performance as measured by these parameters as well as overall response to exercise suggests a potential role for the use of computational simulations as part of the diagnostic follow up regimen. These parameters could also be used in, for example, a simulation-based cost function analysis to best evaluate optimal Fontan design and performance of proposed interventions. In doing so, we hope to lay a foundation for directly linking simulation results with patient outcomes and to provide additional tools for risk stratification and improved outcomes for patients.

Acknowledgments

The authors wish to thank Adam Bernstein, Jessica Shih and Ryan Spilker for assistance with model building and simulations, and Heidi Terwey for assistance with patient recruitment. Support for the Simvascular software package was provided by simtk.org, as well as Dr. Nathan Wilson.

Funding Sources

Alison Marsden was supported by a Burroughs Wellcome Fund Career Award at the Scientific Interface, and by an American Heart Association postdoctoral fellowship and Beginning Grant in Aid award. This work was also supported by the National Science Foundation under grant number 0205741 and the Vera Moulton Wall Center for Pulmonary Vascular Disease at Stanford University.

Disclosures

None.

Corresponding Author: Alison L. Marsden, PhD, Mechanical and Aerosapce Engineering, University of California San Diego, 9500 Gilman Dr., La Jolla, CA 92093-0411, USA. Tel: 858-822-3744; Fax: (858) 534-4543; E-mail: amarsden@ucsd.edu

Conflict of interest: None.

Accepted in final form: December 23, 2009.

References

1 de Leval MR, Dubini G, Migliavacca F, et al. Use of computational fluid dynamics in the design of

surgical procedures: application to the study of competitive flows in cavo-pulmonary connections. *J Thorac Cardiovasc Surg*. 1996;111:502–513.
2 Dubini G, de Leval MR, Pietrabissa R, Montevecchi FM, Fumero R. A numerical fluid mechanical study of repaired congenital heart defects: application to the total cavopulmonary connection. *J Biomech*. 1996;29:111–121.
3 Migliavacca F, Dubini G, Pietrabissa R, de Leval MR. Computational transient simulations with varying degree and shape of pulmonic stenosis in models of the bidirectional cavopulmonary anastomosis. *Med Eng Phys*. 1997;19:394–403.
4 Migliavacca F, Dubini G, Bove EL, de Leval MR. Computational fluid dynamics simulations in realistic 3-D geometries of the total cavopulmonary anastomosis: the influence of the inferior caval anastomosis. *J Biomech Eng*. 2003;125:805–813.
5 Petrossian E, Reddy VM, Collins KK, et al. The extracardiac conduit Fontan operation using minimal approach extracorporeal circulation: early and midterm outcomes. *J Thorac Cardiovasc Surg*. 2006;132:1054–1063.
6 Marsden AL, Vignon-Clementel IE, Chan F, Feinstein JA, Taylor CA. Effects of exercise and respiration on hemodynamic efficiency in CFD simulations of the total cavopulmonary connection. *Ann Biomed Eng*. 2007;35:250–263.
7 Whitehead KK, Pekkan K, Kitahima HD, Paridon SM, Yoganathan AP, Fogel MA. Nonlinear power loss during exercise in single-ventricle patients after the Fontan: insights from computational fluid dynamics. *Circulation*. 2007;116:I–165–I–171.
8 Salvin JW, Scheurer MA, Laussen PC, et al. Factors associated with prolonged recovery after the Fontan operation. *Circulation*. 2008;118:S171–S176.
9 Marino BS. Outcomes after the Fontan procedure. *Curr Opin Pediatr*. 2002;14:620–626.
10 Pike NA, Vricella LA, Feinstein JA, Black MD, Reitz BA. Regression of severe pulmonary arteriovenous malformations after Fontan revision and hepatic factor rerouting. *Ann Thorac Surg*. 2004;78:697–699.
11 Rosenthal DN, Friedman AH, Kleinman CS, Kopf GS, Rosenfeld LE, Hellenbrand WE. Thromboembolic complications after Fontan operations. *Circulation*. 1995;92:287–293.
12 Silvilairat S, Cabalka AK, Cetta F, Grogan M, Hagler DJ, O'Leary PW. Protein-losing enteropathy after the Fontan operation: associations and predictors of clinical outcome. *Congenit Heart Dis*. 2008;3:262–268.
13 DeGroff CG. Modeling the fontan circulation: where we are and where we need to go. *Pediatr Cardiol*. 2008;29:3–12.
14 Wilson N, Wang K, Dutton R, Taylor CA. A software framework for creating patient specific geometric models from medical imaging data for simulation based medical planning of vascular surgery. *Lect Notes Comput Sci*. 2001;2208:449–456.
15 Schmidt JP, Delp SL, Sherman MA, Taylor CA, Pande VS, Altman RB. The Simbios national center: systems biology in motion. *Proc IEEE*, special issue on Computational System Biology. 2008;96:1266–1280.
16 Shachar GB, Fuhrman BP, Wang Y, Lucas RV Jr, Lock JE. Rest and exercise hemodynamics after the fontan procedure. *Circulation*. 1982;65:1043–1048.
17 Giardini A, Balducci A, Specchia S, Gaetano G, Bonvicini M, Picchio FM. Effect of sildenafil on haemodynamic response to exercise capacity in fontan patients. *Eur Heart J*. 2008;29:1681–1687.
18 Hjortdal VE, Emmertsen K, Stenbog E, et al. Effects of exercise and respiration on blood flow in total cavopulmonary connection: a real-time magnetic resonance flow study. *Circulation*. 2003;108:1227–1231.
19 Pedersen EM, Stenbog EV, Frund T, et al. Flow during exercise in the total cavopulmonary connection measured by magnetic resonance velocity mapping. *Heart*. 2002;87:554–558.
20 Sheriff DD, Powell LB, Scher AM. Is rapid rise in vascular conductance at onset of dynamic exercise due to muscle pump? *Am J Physiol*. 1993;265:H1127–H1234.
21 Vignon-Clementel IE, Figueroa CA, Jansen KE, Taylor CA. Outflow boundary conditions for three-dimensional finite element modeling of blood flow and pressure in arteries. *Comput Methods Appl Mech Eng*. 2006;195:3776–3796.
22 Westerhof N, Lankhaar J, Westerhof BE. The arterial windkessel. *Med Biol Eng Comput*. 2009;47:131–141.
23 Spilker RL, Feinstein JA, Parker DW, Reddy VM, Taylor CA. Morphometry-based impedance boundary conditions for patient-specific modeling of blood flow in pulmonary arteries. *Ann Biomed Eng*. 2007;35:546–549.
24 Kulik TJ, Bass JL, Fuhrman BP, Moller JH, Lock JE. Exercise induced pulmonary vasoconstriction. *Br Heart J*. 1983;50:59–64.
25 Marsden AL, Bernstein AJ, Reddy VM, et al. Evaluation of a novel y-shaped extracardiac Fontan baffle using computational fluid dynamics. *J Thocac Cardio Surg*. 2009;137:394–403.
26 Bove EL, de Leval MR, Migliavacca F, Guadagni G, Dubini G. Computational fluid dynamics in the evaluation of hemodynamic performance of cavopulmonary connections after the Norwood procedure for hypoplastic left heart syndrome. *J Thorac Cardiovasc Surg*. 2003;126:1040–1047.
27 Grigioni M, D'Avenio G, Amodeo A, Di Donato RM. Power dissipation associated with surgical operations' hemodynamics: critical issues and application to the total cavopulmonary connection. *J Biomech*. 2006;39:1583–1594.

28 Shadden SC, Taylor CA. Characterization of coherent structures in the cardiovascular system. *Ann Biomed Eng*. 2008;36:1152–1162.
29 Reininger AJ, Reininger CB, Heinzmann U, Wurzinger LJ. Residence time in niches of stagnant flow determines fibrin clot formation in an arterial branching model–detailed flow analysis and experimental results. *Thromb Haemost*. 1995;74:916–922.
30 Zarins CK, Giddens DP, Bharadvaj BK, Sottiurai VS, Mabon RF, Glagov S. Carotid bifurcation atherosclerosis. quantitative correlation of plaque localization with flow velocity profiles and wall shear stress. *Circ Res*. 1983;53:502–514.
31 Tang BT, Cheng CP, Draney MT, et al. Abdominal aortic hemodynamics in young healthy adults at rest and during lower limb exercise: quantification using image-based computer modeling. *Am J Physiol Heart Circ Physiol*. 2006;291:H668–H676.
32 Caro CG, Fitz-Gerald JM, Schroter RC. Arterial wall shear and distribution of early atheroma in man. *Nature*. 1969;223:1159–1161.
33 Moyle KR, Mallinson GD, Occleshaw CJ, Cowan BR, Gentles TL. Wall shear stress is the primary mechanism of energy loss in the Fontan connection. *Pediatr Cardiol*. 2006;27:309–315.
34 Healy TM, Lucas C, Yoganathan AP. Noninvasive fluid dynamic power loss assessments for total cavopulmonary connections using the viscous dissipation function: a feasibility study. *J Biomech Eng*. 2001;123:317–324.
35 Coon PD, Rychik J, Novello RT, Ro PS, Gaynor JW, Spray TL. Thrombus formation after the Fontan operation. *Ann Thorac Surg*. 2001;71:1990–1994.
36 Justino H, Benson LN, Freedom RM. Development of unilateral pulmonary arteriovenous malformations due to unequal distribution of hepatic venous flow. *Circulation*. 2001;103:E39–E40.
37 Figueroa CA, Vignon-Clementel IE, Jansen KE, Hughes TJR, Taylor CA. A coupled momentum method for modeling blood flow in three-dimensional deformable arteries. *Comput Meth Appl Mech Engrg*. 2006;195:5685–5706.
38 Bazilevs Y, Calo VM, Hughes TJR, Zhang Y. Isogeometric fluid-structure interaction: theory, algorithms and computations. *Comput Mech*. 2008; 43:3–37.
39 Zhang Y, Bazilevs B, Goswami S, Bajaj CL, Hughes TJR. Patient-specific vascular NURBS modeling for isogeometric analysis of blood flow. *Comput Methods Appl Mech Eng*. 2007;196:2943–2959.
40 Dasi LP, Pekkan K, Katajima HD, Yoganathan AP. Functional analysis of Fontan energy dissipation. *J Biomechanics*. 2008;41:2246–2252.
41 Taylor CA, Hughes TJR, Zarins CK. Finite element modeling of blood flow in arteries. *Comput Methods Appl Mech Eng*. 1998;158:155–196.
42 Whiting CH, Jansen KE. A stabilized finite element method for the incompressible Navier-Stokes equations using a hierarchical basis. *Int J Numer Methods Fluid*. 2001;35:93–116.
43 Muller J, Sahni O, Li X, Jansen KE, Shephard MS, Taylor CA. Anisotropic adaptive finite element method for modeling blood flow. *Comput Methods Biomech Biomed Eng*. 2005;8:295–305.
44 Fehlberg E. Low-order classical Runge-Kutta formulas with step size control and their application to some heat transfer problems. *NASA Technical Report*. 1969;315.

Appendix: Details of Computational Methods

The purpose of the appendix is to provide further details on the simulations and computational methods for technically-oriented readers. Additional details can be found in Marsden et al.[6] and Taylor et al.[41] The simulations performed in this work used a Newtonian approximation for blood with values of 0.04 g/(cm s) for viscosity 1.06 g/cm^3 for density.[41,42] An anisotropic adaptive meshing scheme[43] was used to ensure mesh convergence using approximately 1.5 million elements for each model.

The respiration model applied at the inflow boundaries was constructed based on Fontan patient data from a real-time imaging study by Hjortdal et al. Polynomial models for inspiration and expiration were constructed following our previous work.[6] This zero-mean respiratory component was then superimposed on the IVC flow waveform (obtained from MRI) for all patients. Based on the IVC diameter at the inflow, the mean Reynolds numbers in the IVC ranged from 340 to 600 at rest and from 1360 to 2380 at heavy exercise. The outflow boundary conditions were prescribed using the coupled multidomain method following the work of Vignon et al.[21]

Post-processing the simulation results yielded energy efficiency, wall shear stress, pressure levels and flow distribution. The energy efficiency was computed as follows. The energy dissipation (neglecting gravitational effects) is given by

$$E_{\text{diss}} = -\sum_{i=1}^{N_{\text{in}}} \int_{A_i} \left(p + \frac{1}{2}\rho u^2\right)\mathbf{u}\cdot d\mathbf{A} - \sum_{i=1}^{N_{\text{out}}} \int_{A_i} \left(p + \frac{1}{2}\rho u^2\right)\mathbf{u}\cdot d\mathbf{A}, \quad (1)$$

where u is the velocity, p is the pressure, ρ is the density, N_{in} and N_{out} are the number of model

inlets and outlets, respectively, and A_i is the area of the i^{th} inlet or outlet. The energy efficiency is then

$$E_{\text{effic}} = E_{\text{out}}/E_{\text{in}}, \quad (2)$$

where E_{in} is the first term in equation (1) and E_{out} is the second term. The efficiencies we report in this work are the time-averaged values over one respiratory cycle. Convergence studies confirmed that results did not change using multiple respiratory cycles. Efficiency values were computed from the simulation results in a post processing step.

IVC flow distribution was computing using a Lagrangian particle tracking method.[28] The inlet of the IVC was uniformly seeded with 35 000 particles every 1/50th of the respiratory cycle for an entire cycle. Particles were assumed to be massless, and effects of diffusion were neglected due to the short residence time of the particles in the computational domain. The advection scheme employed a Runge-Kutta-Fehlberg[44] integration algorithm with a maximum error tolerance of 10^{-5} and a linear interpolation of the velocity data in space and time.